Journal of Rock Mechanics and Geotechnical Engineering 14 (2022) 1042–1051

Contents lists available at ScienceDirect

Journal of Rock Mechanics and Geotechnical Engineering

journal homepage: www.jrmge.cn

Full Length Article

Bio-inspired vibrational wireless underground communication system

Yi Zhong, Junliang (Julian) Tao*

Center for Bio-mediated and Bio-inspired Geotechnics, School of Sustainable Engineering and the Built Environment, Arizona State University, Tempe, AZ, 85287, USA

ARTICLE INFO

Article history:
Received 14 January 2022
Received in revised form
19 May 2022
Accepted 14 June 2022
Available online 28 June 2022

Keywords:
Bio-inspired vibration
Underground communication
Seismic wave
Wireless communication
Internet of underground things (IoUT)

ABSTRACT

The internet of the underground things (IoUT) is an emerging field that concerns connected underground sensing nodes and can find applications in various fields such as geotechnical engineering, precision agriculture, and search and rescue operations. The complex underground environment and multiphase nature of the soil pose challenges to wireless underground communication. Most existing studies on wireless underground communication focus on the use of electromagnetic waves. However, as a highly lossy material for electromagnetic waves, soil can limit the range and reliability of data transmission. Inspired by subterranean animals that rely on vibrations or seismic waves for underground communication, the prototype system developed in this study is based on vibration. This system includes a bio-inspired vibrating source, a micro-electromechanical system (MEMS) accelerometer, a microcontroller, and a set of algorithms for encoding and decoding information. Specifically, the mole rats-inspired source is small in size, low in cost, and energy-efficient. An on-off-keying decoding algorithm enhanced with an error-correction algorithm is found to be robust in transmitting textual and imaginary information. With the current design, a maximum transmission bit rate of 16–17 bits per second and a transmission distance of 80 cm can be achieved. The bit error ratio is as low as 0.1%, demonstrating the robustness of the algorithms. The performance of the developed system shows that seismic waves produced by vibration can be used as an information carrier and can potentially be implemented in the IoUT.

1. Introduction

The internet of underground things (IoUT) aims to provide remote underground sensing and monitoring, and it has been widely applied in the field of geotechnical site investigation, precision agriculture (Vuran et al., 2018a, b; Salam and Shah, 2019a), mine/reservoir monitoring (Sun and Akyildiz, 2010a, b), underground infrastructure monitoring (Salam and Shah, 2019b; Raza and Salam, 2020), landslide monitoring (Ramesh, 2014), and localization (Lin et al., 2017). The IoUT mainly consists of two components entirely or partially buried in soils: sensor nodes and communication modules. The sensor nodes collect relevant information about the underground environment, including soil composition, moisture content, temperature, and pore water pressure, etc. By interconnecting sensors with communication modules, real-time or near real-time data acquired from the field can be sent through the soil and eventually received by the end users.

The performance of the underground communication modules is crucial to the success of the IoUT system. Like the conventional above-ground Internet of Things (IoT), communication among sensing nodes of an IoUT can be achieved with or without transmission wires. However, the complexity and cost of installation and maintenance of transmission wires would grow drastically with the number of the sensing nodes and the embedment depth. Therefore, the wireless option is more attractive for an IoUT, and the focus of this paper is on wireless underground communication (WUC).

Conventional wireless IoT system relies on through-air communication, mainly using electromagnetic (EM) waves. WUC can also be transmitted through the air in some scenarios, such as in mines and tunnels. But for most IoUT applications, through-soil communication is unavoidable (Saeed et al., 2019). The heterogeneous nature of the soil, in which the soil composition varies with space and time, poses challenges to the success of underground wireless communication based on EM waves. As a result, the

* Corresponding author.
E-mail address: jtao25@asu.edu (J. Tao).
Peer review under responsibility of Institute of Rock and Soil Mechanics, Chinese Academy of Sciences.

https://doi.org/10.1016/j.jrmge.2022.06.005

transmission range and effectiveness of EM waves in soil are limited (Akyildiz and Stuntebeck, 2006). In addition, large antennas are typically required to transmit and receive EM waves (Sun and Akyildiz, 2010b), which makes the installation process challenging. Alternatively, a recently proposed underground communication system based on magnetic induction (MI) overcomes some drawbacks of EM-based techniques (Sun and Akyildiz, 2010a, b; Lin et al., 2017). There are no significant differences in magnetic permeabilities between solid particles, water, and air; thus, the underground conditions cause little variations in the attenuation rate of the magnetic fields, and the MI channel is more robust to the underground environment than the channel for EM-based techniques. Moreover, the MI technique could also address the need for a large antenna by using a small coil of wire. However, the receiving power loss of the MI-based communication technique is a sixth-order function of the transmission range, indicating high path loss and a limited range of transmission (Sun and Akyildiz, 2010a). Using relay points can significantly reduce the path loss. But this limits the practicality and poses challenges for installation of the multiple nodes in field, especially it requires short distance between relay points (typically 1 m).

In this study, an alternative WUC technique based on a mechanical wave approach inspired by subterranean animals is explored. Most subterranean animals and some surface-dwelling animals rely on vibrations for intraspecific communication, localization of prey, and detection of predators (Hill, 2001). It is conservatively estimated that over 230,000 arthropods species and a great number of vertebrates use substrate-borne vibrations for communication (Cocroft et al., 2014). One prominent example is the long-distance communication (as far as 16 km) used by Asian elephants, who are able to generate seismic waves when moving and can detect vibrational signals through somatosensory receptors (O'Connell-Rodwell, 2007). Although small animals cannot generate seismic waves that are as strong as those of elephants, they can still achieve long-distance underground communication using seismic cues. For example, spalacid mole-rats generate rhythmic, substrate-borne vibrational signals by thumping their heads against the ceilings of their tunnels. By doing this, these blind mole-rats are able to transmit information across many meters between territories (Heth et al., 1987; Nevo et al., 1991).

Utilizing seismic waves is not new in geotechnical engineering and geophysics. Vibration-based testing methods, such as seismic reflection, seismic refraction, and surface wave measurements, are widely used to characterize subsurface conditions and to determine design parameters (Stokoe and Santamarina, 2000). Nevertheless, the potential of using seismic waves to carry information in communication systems has not been widely explored. The earliest documented study described a large thumping type transducer, which was mounted on a hilltop to induce seismic cues and was used to communicate with devices placed in an underground mine (Ikrath and Schneider, 1968). However, only unidirectional communication was allowed, and the data rates were low. More recently, a small-sized underground communication system that uses acoustic waves was proposed (Yang et al., 2020). In general, the concept of using mechanical waves for WUC has been validated; however, there is still room to improve the efficiency and effectiveness of such as system.

The objective of this study is to develop a small-size, energy-efficient, and cost-effective vibration-based WUC system that can be used for IoUT applications. The following sections describe the components of the developed system, including a bio-inspired source, communication channel characteristics, receivers, and the encoding/decoding algorithms, as well as how the system performance is evaluated through laboratory tests.

2. System design and description

Communication is the process of transferring information from a transmitter to a receiver. In a typical communication system, the input message which consists of texts, numbers, and/or images is first encoded and then converted into a source signal. Then it travels through the communication channel and is picked up by the receiver; the received signals are then decoded, and the message is restored. The schematic diagram in Fig. 1 highlights the major components of the proposed WUC system, including soil as the communication channel, a bio-inspired vibrational transmitter, and accelerometers as receivers. In the proposed communication system, messages, including text files and images, are first converted into binary streams. The binary streams are then translated into a series of vibrations generated by the developed transmitter. The vibrations travel through soil in the form of seismic waves and are picked up by accelerometers. The received signals are translated into binary streams and converted back to text files or images.

2.1. Communication channel characteristics

Soil is a multiphase system that consists of solid particles, water, and air. It allows the propagation of both compression and shear seismic waves. The propagation of a seismic wave is primarily determined by transmission loss, noise, reflection, refraction, and tempo-spatial variability of the soil channel. Transmission loss and noise are the principal factors that determine the transmission range and the signal-to-noise ratio (SNR). The spatio-temporal variability, as well as the multipath propagation can influence the seismic signal design and processing, design of the architecture of the communication system, and performance of the system.

Transmission loss is caused by geometric attenuation, material loss or intrinsic attenuation, and apparent attenuation (Santamarina et al., 2001). As the wavefront propagates, its size increases, causing a decrease in the wave amplitude with distance. Scattering, frictional losses due to particle contacts, as well as viscous losses due to the relative movement between the solid particles and fluid are responsible for material attenuation. Partial transmission and mode convention caused by the presence of the interface can also cause wave amplitude to decrease. Total attenuation of seismic waves depends on the degree of saturation, bulk density, stiffness of the granular skeleton, and bulk modulus of the fluid.

In general, soil is inhomogeneous with irregular boundaries, and its characteristics vary with time and space. Reflection and refraction from soil layers can cause multipath propagation, which may result in inter-bit interference in a single-carrier digital communication system. As the degree of saturation is affected by rainfall, sunlight, and temperature, it may vary with time. Consequently, the time variability of soil properties can affect seismic wave attenuation. In addition, soil properties and soil profiles show spatial variation. The geometry of multipath propagation and its spatio-temporal dependence are especially important for a moving communication system.

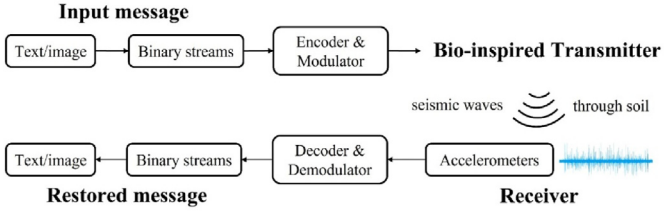

Fig. 1. Schematic of the developed bio-inspired underground communication system.

The effective transmission distance of seismic waves is limited not only by the attenuation phenomena but also by the noise level, as the noise level affects SNR and limits the transmission range and effectiveness of the signal. Noise observed in the underground environment consists of artificial noise and ambient noise. Artificial noise occurs near the ground surface and results from transportation and industry activities, and it significantly increases the noise level in this region. Most ambient noises are generated by environmental activities of natural processes. The characteristics of the communication channel require that the encoded signals generated by the source are insensitive to ambient noises and that the receivers are sensitive enough to accommodate various types of signal attenuation.

2.2. Bio-inspired source design

To generate reliable seismic waves, animals use a variety of methods, including drumming (striking), tremulation (vibrating the entire body), stridulation (rubbing), and tymbal buckling (Hill, 2001; Hill et al., 2019). Drumming describes the behavior where body parts are used to strike the substrate in a percussive fashion. Although drumming produces broadband signals, the soil will filter the signals, causing spectral differences at the receiver's end. Consequently, in drumming-induced vibrational signals, the temporal patterns are more important than the spectral details. Subterranean mammals that utilize drumming include spalacid mole-rats, Cape mole-rats, and African mole-rats (Nevo et al., 1991; Narins et al., 1992; Ema, 2012). The typical body length of a mature specimen of these blind mole-rats is from 10.5 cm to 16.5 cm, and their vibration communications have a range of several meters. Considering their small body size and the transmission range, these blind mole-rats employ an energy-efficient and effective method for underground communication. Tremulation describes the behavior where an animal vibrates its entire body against a substrate. Many species of termites (e.g. *Coptotermesformosanus*, *Retkulitermes speratus*, *Zootermopsis nevadensis*) shake themselves back and forth or right and left against the nest walls for communication purposes, and the frequency of the tremulation is around 25 Hz (Ohmura et al., 2009). Stridulation and tymbal buckling are mainly used by insects and involve vibration against plant parts. Since this study concerns vibrations through soils, the inspirations for the wave sources in the proposed system were mainly drawn from tremulation and drumming.

Inspired by drumming and tremulation, two small-size, low-cost, energy-efficient, and controllable vibrational sources were designed and fabricated (Fig. 2). The drumming-inspired source consists of two push-pull solenoids (Adafruit 413) encased in a three-dimensional (3D) printed box. The solenoids are characterized by a 6 N striking force at 12 V of direct current (VDC) and a push or pull-type throw of 10 mm (Fig. 2a). When activated, the plunger of the solenoids moves out of the solenoid's body and strikes the 3D-printed box. When powered off, the plunger moves back to its original position due to the return force provided by the spring. The tremulation-inspired source consists of a micro vibration motor (8 mm in diameter and 15 mm in length), which is encased in an acrylic tube (Fig. 2b). The eccentric weight on the rotating shaft of the vibration motor generates centrifuge force when it rotates. When the vibration motor is activated, the induced unbalanced force results in whole body vibration.

To control the drumming or tremulation–induced vibrations, a microcontroller (Arduino Uno 3) and a motor driver (Adafruit v2.3) were used to convert the encoded binary streams and to regulate the voltage input to the solenoids or vibration motors. The accelerometers at the receiving ends were also connected to the microcontroller for data collection.

2.3. Receivers

Coil-based geophones and micro-electromechanical systems (MEMS) accelerometers are two major sensors used for acquiring seismic data. Geophones, a proven technology, usually do not require a power supply and can provide reliable velocity measurements. While geophones were mainly used in an earlier preliminary study (Zhong et al., 2021), MEMS accelerometers have many attractive attributes when compared with geophones.

MEMS sensors are small and light in weight. Nowadays, a high-performance triaxial MEMS accelerometer can be much less than 1 cm × 1 cm and weigh less than 1 g. The small size and highly integrated nature of MEMS sensors enable them to be implemented with other IoUT devices such as underground self-burrowing robots (Tao et al., 2020). MEMS accelerometers work below their resonant frequency, while geophones work above their resonant frequency. The resonant frequency of MEMS accelerometers is far above the seismic band, which makes it possible to record low-frequency signals (below 10 Hz) using MEMS accelerometers without attenuation. MEMS accelerometers can measure accelerations in three directions, while standalone geophones can only measure velocity in the direction along the axis of the coil. In addition, the gravity vector measured by the MEMS accelerometers

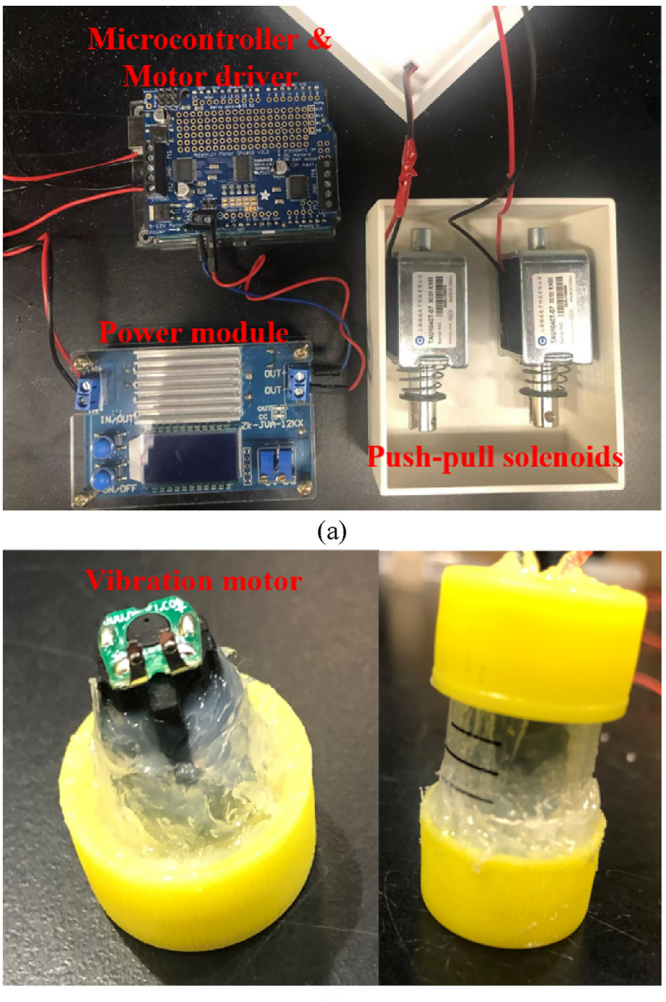

Fig. 2. Bio-inspired vibration sources: (a) Drumming-inspired vibrational source based on push-pull solenoids; and (b) Tremulation-inspired vibrational source based on a vibration motor.

also provides a reference for sensitivity calibration and tilting measurement.

MEMS accelerometers were chosen as receivers in the proposed system due to their small size, better performance for recording low-frequency seismic signals, and their ability to obtain multi-directional and tilting measurements. In this study, the MEMS accelerometer MMA8452Q (NXP Semiconductors N.V., Netherlands) was selected based on its small size and low-power requirements. This triaxial capacitive MEMS accelerometer has a dynamically selectable full-scale (±2 g/±4 g/±8 g), a 12-bit digital output, and a sampling rate up to 800 Hz.

2.4. Coding and modulation

The vibrations generated by the sources have to be controlled to contain information to be transmitted. The process of translating information (such as a string of numbers and letters) into a series of vibrations is called encoding and modulation, which describes the process whereby the frequency, amplitude, and/or phase of the vibrations are changed.

Mole-rats are able to encode their biological information into seismic waves by changing the impulse amplitude and the time interval between impulses (Rado et al., 1987), as can be noticed in the bursts shown in Fig. 3. These mole-rats seem to use the most straightforward modulation scheme, which is called amplitude shift keying. On-off keying (OOK), which is the simplest form of amplitude shift keying, is used in this study to modulate the signal from the bio-inspired vibrational sources. In this binary modulation scheme, the presence of a signal for a specific duration represents "1", while the absence of the same duration "0".

Before being modulated using OOK, different types of messages (text, numbers, and images) need to be converted to binary streams. In information processing and communication, coding is a system of rules that are used when converting information to another form. In the encoding process, messages are converted into binary streams, while the reverse process (decoding) is used once the message is received. One of the most straightforward and well-known codes is Morse code. Our preliminary study showed that messages could be encoded using Morse code and then carried by modulated seismic waves for underground communication (Zhong et al., 2021). However, Morse code is a variable-length code and can only represent numbers and letters, but no special characters. To encode plain text in the proposed system, we selected Baudot–Murray code, a 5-bit coding method. The 5-bit series used to encode a character is also called a byte. The Baudot-Murphy code, or the International Telegraph Alphabet No. 2 (ITA2) code was introduced by Consultative Committee for International Telegraphy and Telephony or CCITT (now known as ITU-T, or Telecommunication Standardization Section of the International Telecommunications) in 1924 and the mapping between a character and a binary representation is usually presented as a table (Bruchanov, 2005). Baudot–Murray code can represent two sets of characters (one for letters and another for numbers and punctuation) using a series of 5-bit with the help of shift codes. For example, the string "CBBG" can be encoded as "11111 01110 11001 11001 11010", and the string "CBBG 2021" can be encoded as "11111 01110 11001 11001 11010 00100 11011 10011 10110 10011 10111". The bytes "11111" and "11011" are shift codes, "11111" represents the letter set of characters while "11011" indicates the number and punctuation set of characters.

In addition, Hamming (7, 4) code is implemented in the proposed system to increase its robustness. Hamming code is an error correction code that can be used to autocorrect error bits. By adding three parity bits to 4-bits of data, this algorithm allows the correction of 1-bit errors without the detection of uncorrected errors. The Hamming code process can be understood as a mathematical translating process based on three matrices: the code generating matrix $\boldsymbol{G}^{\mathrm{T}}$, parity-check matrix $\boldsymbol{H}$, and decoding matrix $\boldsymbol{R}$.

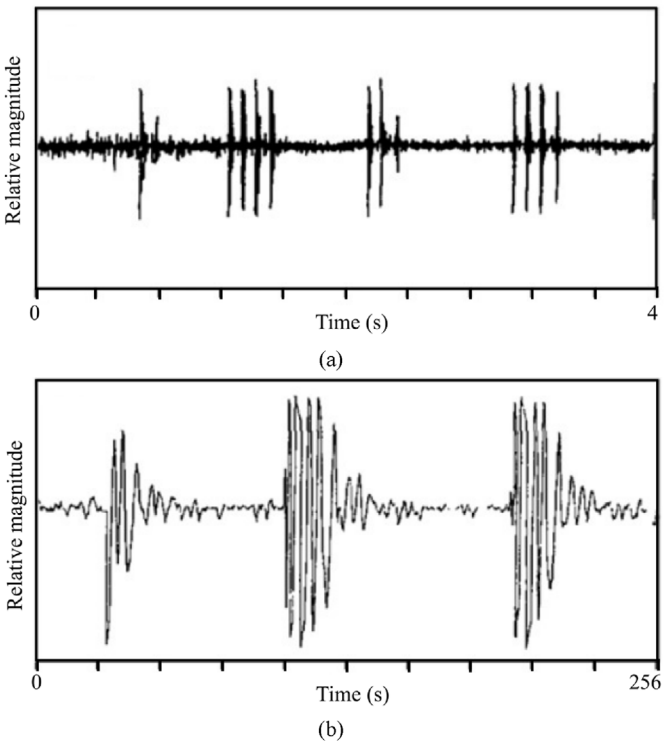

Fig. 3. Temporal pattern of mole-rat head drumming in nature picked by a vertical geophone (the plots are directly reproduced from Rado et al., 1987): (a) Consecutive bursts performed by an individual mole rate; and (b) Individual head drums on an expanded time scale.

$$\boldsymbol{G}^{\mathrm{T}} = \begin{bmatrix} 1 & 1 & 0 & 1 \\ 1 & 0 & 1 & 1 \\ 1 & 0 & 0 & 0 \\ 0 & 1 & 1 & 1 \\ 0 & 1 & 0 & 0 \\ 0 & 0 & 1 & 0 \\ 0 & 0 & 0 & 1 \end{bmatrix} \tag{1a}$$

$$\boldsymbol{H} = \begin{bmatrix} 1 & 0 & 1 & 0 & 1 & 0 & 1 \\ 0 & 1 & 1 & 0 & 0 & 1 & 1 \\ 0 & 0 & 0 & 1 & 1 & 1 & 1 \end{bmatrix} \tag{1b}$$

$$\boldsymbol{R} = \begin{bmatrix} 0 & 0 & 1 & 0 & 0 & 0 & 0 \\ 0 & 0 & 0 & 0 & 1 & 0 & 0 \\ 0 & 0 & 0 & 0 & 0 & 1 & 0 \\ 0 & 0 & 0 & 0 & 0 & 0 & 1 \end{bmatrix} \tag{1c}$$

For example, a 4-bit vector $\boldsymbol{p} = (1 \quad 1 \quad 1 \quad 1)^{\mathrm{T}}$ is shown in a vector column, and can be encoded into 7-bits transmitted code $\boldsymbol{x}$ by taking the product of $\boldsymbol{G}$ and $\boldsymbol{P}$ followed by an operation of entries modulo 2:

$$\boldsymbol{x} = \boldsymbol{G}^{\mathrm{T}}\boldsymbol{p} = \begin{bmatrix} 1 & 1 & 0 & 1 \\ 1 & 0 & 1 & 1 \\ 1 & 0 & 0 & 0 \\ 0 & 1 & 1 & 1 \\ 0 & 1 & 0 & 0 \\ 0 & 0 & 1 & 0 \\ 0 & 0 & 0 & 1 \end{bmatrix} \begin{Bmatrix} 1 \\ 1 \\ 1 \\ 1 \end{Bmatrix} = \begin{Bmatrix} 3 \\ 3 \\ 1 \\ 3 \\ 1 \\ 1 \\ 1 \end{Bmatrix} (\mathrm{mod}\ 2) = \begin{Bmatrix} 1 \\ 1 \\ 1 \\ 1 \\ 1 \\ 1 \\ 1 \end{Bmatrix} \tag{2}$$

When there is an error (for example, the received code is $\boldsymbol{r} = \{1\ \ 1\ \ 1\ \ 1\ \ 1\ \ 0\ \ 1\}^{\mathrm{T}}$) compared with the transmitted code $\boldsymbol{x}$, the error can be located using the parity-check matrix:

$$\boldsymbol{Hr} = \begin{bmatrix} 1 & 0 & 1 & 0 & 1 & 0 & 1 \\ 0 & 1 & 1 & 0 & 0 & 1 & 1 \\ 0 & 0 & 0 & 1 & 1 & 1 & 1 \end{bmatrix} \begin{Bmatrix} 1 \\ 1 \\ 1 \\ 1 \\ 1 \\ 0 \\ 1 \end{Bmatrix} = \begin{Bmatrix} 4 \\ 3 \\ 3 \end{Bmatrix} (\mathrm{mod}\ 2)$$

$$= \begin{Bmatrix} 0 \\ 1 \\ 1 \end{Bmatrix} \tag{3}$$

The vector $\boldsymbol{Hr}$ is the same as the sixth column of the parity-check matrix, indicating that the error happens at the sixth bit. The error bit can then be corrected. The decoding process is similar to the encoding process, but by taking the product of $\boldsymbol{R}$ and received bits after the correction $\boldsymbol{r}_{\mathrm{c}}$:

$$\boldsymbol{Rr}_{\mathrm{c}} = \begin{bmatrix} 0 & 0 & 1 & 0 & 0 & 0 & 0 \\ 0 & 0 & 0 & 0 & 1 & 0 & 0 \\ 0 & 0 & 0 & 0 & 0 & 1 & 0 \\ 0 & 0 & 0 & 0 & 0 & 0 & 1 \end{bmatrix} \begin{Bmatrix} 1 \\ 1 \\ 1 \\ 1 \\ 1 \\ 1 \\ 1 \end{Bmatrix} = \begin{Bmatrix} 1 \\ 1 \\ 1 \\ 1 \end{Bmatrix} \tag{4}$$

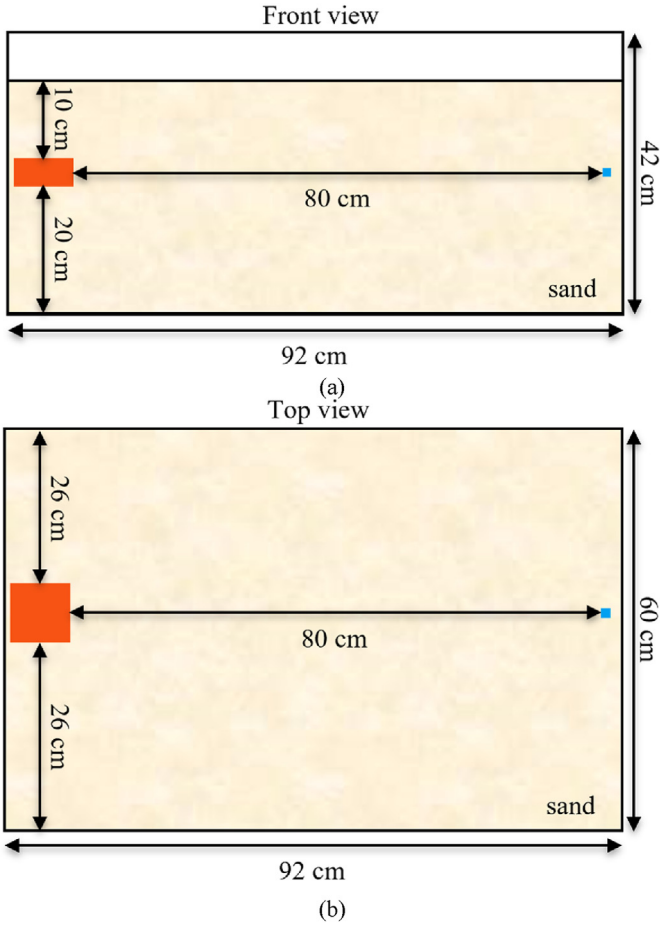

Fig. 4. Experimental setup: (a) Front view and (b) Top view. The orange block on the left in both subfigures indicates the drumming-inspired vibration source, while the blue block on the right indicates the accelerometer.

Both the Baudot-Murphy ITA2 code and the hamming code were implemented in a python script, which was then interfaced with the microcontroller.

2.5. Evaluation test setup

The performance of the bio-inspired vibration sources, as well as the entire WUC system, was evaluated in an acrylic tank having inside dimensions of 92 cm in length, 60 cm in width, and 42 cm in height. Dry Ottawa F65 sands were poured into the tank and tamped to achieve a final global relative density of 45%. When the sand thickness reached 20 cm, the vibration sources and the receiver were placed. More layers of sand were then poured and tamped until the vibration sources and the accelerometer were embedded at a depth of 10 cm (Fig. 4).

The limited size of the sand box may indeed cause reflections of mechanical waves from the boundaries. It is extremely challenging to eliminate all the reflections from the boundaries. In this study, efforts were made to reduce the reflections in the transmitter-receiver direction, especially at the receiver end. A circular hole with 5 cm diameter was cut on the receiver side of the tank, and this hole was then covered using a piece of geotextile which was flexible and was able to absorb the mechanical energy and to prevent wave reflections.

3. Results

3.1. Source and channel evaluation

3.1.1. Qualitative evaluation

The performance of the two bio-inspired vibrational sources was first evaluated qualitatively. An input signal was generated as a square wave with a high amplitude of 3 V, a low amplitude of 0 V, and a duty cycle of 50%, as shown in Fig. 6a. The accelerometer was set initially 5 cm away from the sources. The distance between the accelerometer and the sources was increased gradually if the raw accelerometer data still appeared clear in x- (along the length of the tank), y- (along the width of the tank) or z- (vertical) direction (Fig. 5). For both vibration sources, all components of the accelerations were found to decrease with the distance between the source and the sensor. As the change in accelerations in z-direction was higher than that in the other two directions due to the shallow embedment depth, only the z component of the acceleration was analyzed and reported in this paper.

The two vibration sources showed distinct differences in terms of the acceleration signals. At a distance of 70 cm from the vibration source, the acceleration signals produced by the tremulation-inspired source remained measurable. However, it became difficult to recognize the signal pattern from the raw signal as the SNR level dropped below 1.2 (Fig. 6b). To improve the SNR, a band filter of 60–80 Hz was applied to the raw signal based on the result of a wavelet transform analysis. However, the filtered signal clearly shows the same pattern as in the input (Fig. 6). With the drumming-inspired source, the raw acceleration signals were

always clear enough so no filter was needed to process the data further (see Fig. 7).

Another drawback of the tremulation-inspired source is that the vibrations of the source are suppressed when the source is embedded below 15 cm, due to the relatively high confining pressure and low output torque of the micromotor. The drumming-inspired source does not suffer from this problem, since the solenoids are encased in a large box and the plungers will always impact the inner wall of the box. Therefore, in the subsequent quantitative evaluation of the vibration source and the evaluation of the proposed system, only the drumming-inspired source was considered.

3.1.2. Quantitative evaluation of the vibration sources

To quantitatively evaluate the attenuation of the generated seismic waves, different input voltages (9 V, 10.5 V and 12 V) were supplied to activate the source while the source-to-sensor distance was changed from 5 cm to 80 cm gradually. The solenoids in the vibration source were activated under each input voltage, and activation lasted for 40 ms. Subsequently, the plungers struck the 3D-printed case five times, and sufficient time (about 20 s) was allowed between activations so that subsequent impacts were not affected by the previous ones.

At the maximum source-to-sensor distance of 80 cm, which was limited by sand tank dimensions, the signals remained clear at an input voltage of 9 V. Since a higher input voltage results in a higher impacting force for the solenoids, stronger seismic waves were produced, as expected (Fig. 7a). In terms of each activation, the amplitudes of each individual impulse were found to be consistent (Fig. 7b). The pattern of the induced seismic wave resembled patterns of those produced by mole-rats for underground communication (Fig. 3).

The amplitude–distance relationship for the source with different input voltages under the mentioned experimental setup is plotted in Fig. 8. The dissipation of the waves is mainly attributed to geometric attention, material loss, and scattering.

Geometric attenuation corresponds to the decrease in amplitude with distance due to an increase in the size of the wavefront. Auersch and Said (2010) proposed that a power law can be used to describe the attenuation of a seismic wave with distance:

$$A \propto r^{-q} \tag{5}$$

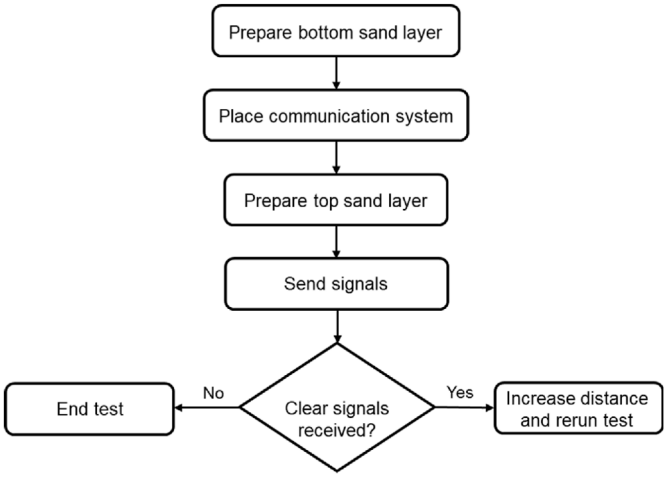

Fig. 5. Schematics of experiment setup and test process.

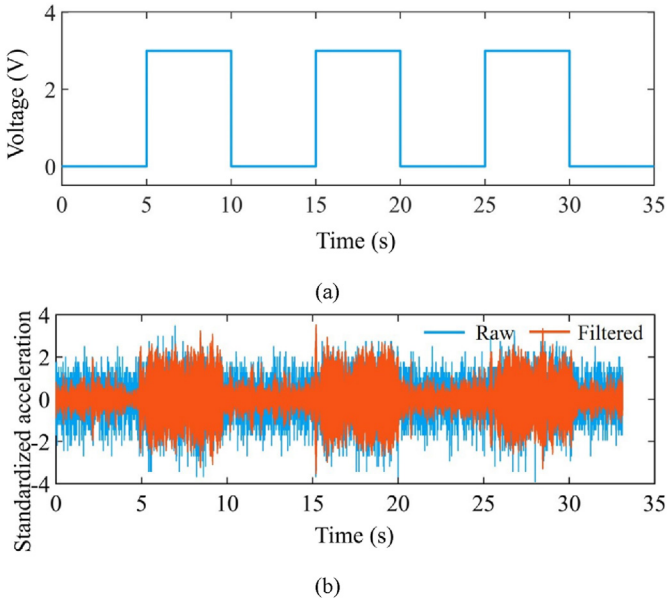

Fig. 6. Qualitative evaluation of the tremulation-inspired vibrational source: (a) Periodic "on-off" signal input; and (b) Raw and filtered signals as received by an accelerometer embedded at the same depth but at a distance of 70 cm from the source.

where A is the acceleration amplitude, r is the distance from the source, and q is the attenuation exponent. For example, the attenuation exponent for geometric attenuation of cylindrical elastic waves is 0.5.

The effect of material loss can be described using an exponential law:

$$A \propto e^{-\alpha r} \tag{6}$$

where α is the attenuation coefficient due to material damping.

Similar to the effect of material damping, scattering attenuation also follows an exponential law. Attenuations due to both material damping and scattering are frequency-dependent, i.e. the attenuation becomes stronger as the frequency increases. Considering all frequency component of a broadband vibration, the mean attenuation caused by material damping and scattering tends to follow a power-law (Auersch, 2010; Auersch and Said, 2010). Therefore, combing the effect of frequency-independent geometric attenuation, material attenuation and scattering, the overall attenuation tends to follow a power law for a broadband vibration.

The vibration induced by the drumming-inspired source is a series of impulses and is therefore considered to be a broadband signal. The amplitude–distance relationship for the vibration source is thus expected to follow a power law (Fig. 8). The best-fitting attenuation exponent for the drumming-inspired vibrational source under the described experimental setup is found to be $q = 0.63$, which is similar to the one reported by Auersch and Said (2010) for vibratory compaction ($q = 0.7$) in the field. The difference can be caused by the difference in soil types and conditions and this particular fitting curve is only valid to the testing condition reported here.

3.2. System evaluation

The performance of the underground communication system was evaluated through two demonstrations: one using a simple text file, and the other using an image file. More details about each

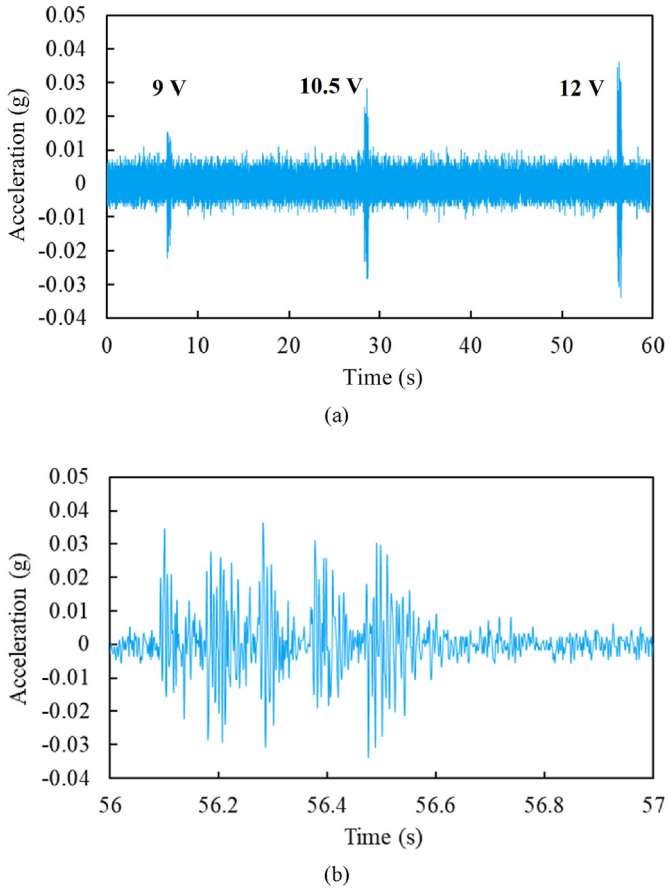

Fig. 7. Sample signals as measured by the accelerometer placed 80 cm away from the source. The embedment depth of the source and accelerometer is 15 cm: (a) Responses under different excitation voltage levels; and (b) Response under an excitation voltage of 12 V on an expanded time scale.

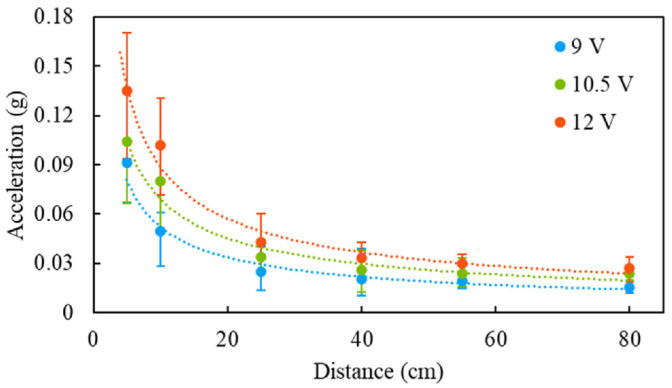

Fig. 8. The acceleration response with distance from the drumming-inspired vibrational source and input voltage.

demonstration and the corresponding results are presented in the following subsections.

3.2.1. Demonstration with a simple text file

To demonstrate the effectiveness of the whole proposed communication system, a text file was first transmitted through dry sand. The source and the accelerometer were placed 70 cm apart at a depth of 10 cm. The plain text file contained the following information: "The current water temperature is 20 °C. The relative density of sand is fifty percent." The plain text was first encoded into binary streams using the Baudot–Murry code and the Hamming code. To facilitate determination of the start and end of the file, a unique binary pattern was inserted before and after the converted binary stream for the text (Fig. 9b). The overall binary stream was sent to the microcontroller to regulate the on/off state of the source. Again, binary "1" corresponds to the activation of the solenoids and results in the compaction of the plunger on the box, while a binary "0" represents the off state and the deactivation of the solenoids.

The time required for two solenoids to complete a push–pull cycle was around 60 ± 10 ms. To minimize the impact of push–pull cycle period uncertainties and to avoid the inter-byte interference (between characters) caused by multipath propagation, a guard interval or guard time was introduced. The guard time corresponds to the time between two consecutive bytes. A greater guard interval time will result in cleaner signal but would also increase the overall transmission time, while a too-small guard interval time may not eliminate the overlap or interferences between two consecutive impacts. In this work, the guard interval of 40 ms is estimated based on the mechanical performance of the solenoids. Uncertainties exist in the mechanical control of the transmitter. During the calibration process, we observed that the average time for the solenoids to complete a push-pull cycle was about 60 ms, with a standard deviation of about 10 ms. The guard interval time was chosen to be 4 times of the standard deviation to ensure that the potential interferences between consecutive impacts are eliminated.

The raw acceleration data recorded by the accelerometer are shown in Fig. 9a. When decoding the recorded signals, the signals between the starting and ending patterns were first identified and then intervening signal was automatically divided into subsequences. Each subsequence window includes one bit and represents a binary "1" or "0". In each subsequence window, if the signals exceed a preset threshold, a binary "1" will be registered; otherwise, a binary "0" is registered (Fig. 9b). The selection of the threshold could affect the decoding quality: a threshold that is too high may leave some impulses undetected, while a threshold that is too low may mistake background noise as impulses. Since the received signals were clear and SNR was high when using the drumming-inspired source, the selection of an appropriate threshold value was straightforward. In this study, the threshold was set as two times the maximum amplitude of the background noise.

As shown in Fig. 9b, the Hamming code is first decoded: each 7-bit sequence is decoded into a 4-bit sequence. As an example, the starting series, "1 1 1 1 1 1 1", "0 1 1 1 1 0 0", and "0 1 0 1 0 1 0" were decoded as "1 1 1 1", "1 1 0 0", and "0 0 1 0" respectively. Next, the Baudot–Murray code is decoded into characters: each 5-bit sequence is decoded into a character. In the above example, "1 1 1 1 1" indicates a letter set, and the subsequent bit sequence "1 1 0 0 0" was decoded as the letter "T" (Fig. 9). After decoding the binary stream into a series of characters, the plain text message was perfectly restored.

3.2.2. Performance comparison with an image file

To further illustrate the performance of the source, the encoding/decoding algorithms and the developed underground communication system (60 pixel × 30 pixel) portable network graphics (PNG)–encoded image (Fig. 10a) was transmitted using the same experimental setup when incorporating different hardware or software design options. The evaluation included six cases, and the parameters are summarized in Table 1.

For each case, four parameters were used to quantify the system performance: the bit error rate (BER), the bit rate, power, and

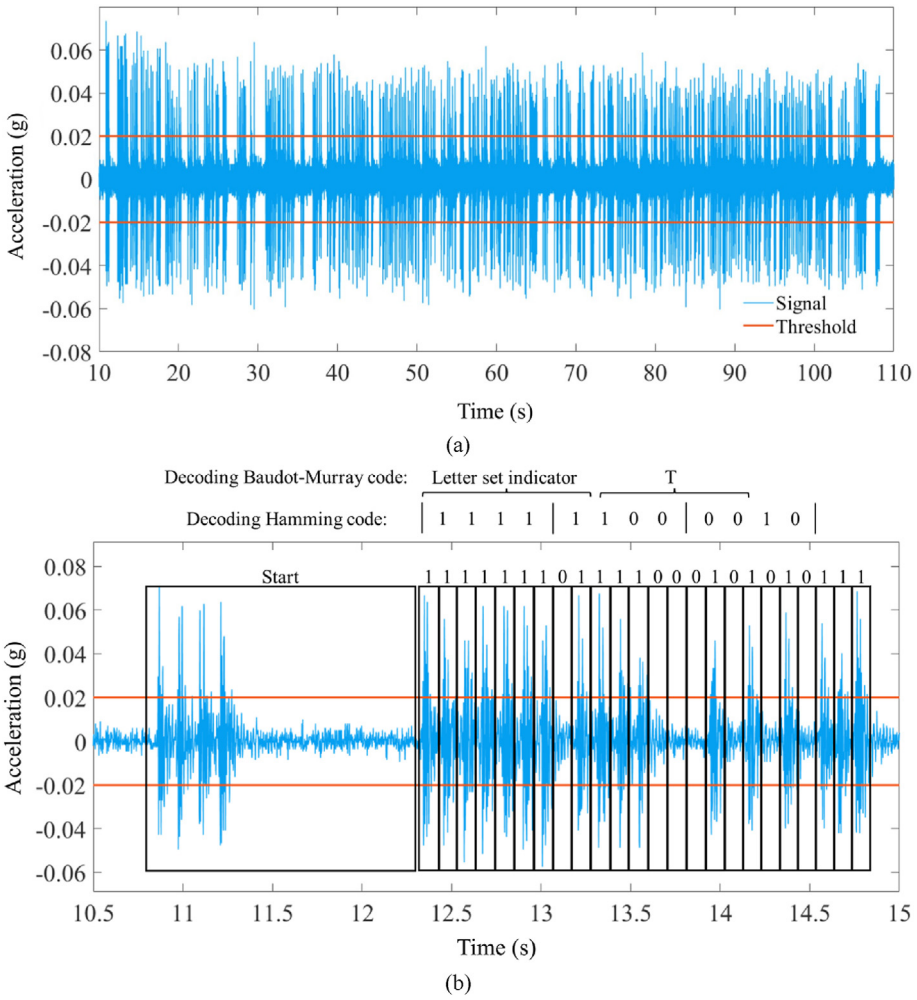

Fig. 9. Demonstration of the decoding algorithm: (a) Received raw signal of a plain text file sent through sand; the threshold used to identify the "on" state is indicated by red lines; and (b) The decoding of the starting segment of the signal. The starting pattern and the restored binary codes are highlighted.

transmission time. The BER is defined as the number of error bits normalized by the total number of bits, and the bit rate is the number of bits per second (bps). The power is evaluated based on the output of the power supply. The transmission time is the duration of file transmission. The restored images for each case are presented in Fig. 10, and the performance metrics are compared in Table 2.

The effectiveness of the Hamming code was explored by transmitting two image binary streams: one with the implementation of the Hamming code and the other without. An apparent difference between restored images was observed (Fig. 10b and c) vs. Fig. 10f and g). By applying an error correction, the BER dropped significantly (Table 2) and the quality of the restored images was much better. A downside of implementing Hamming code is that it required more bits to be sent, resulting in higher energy consumption and a longer transmission time (Table 2).

The bit rate of the developed system is limited by the mechanical operation of the solenoids and the length of guard interval. One solenoid required approximately 60 ms to complete a push-pull cycle, while two solenoids took several milliseconds more. The highest bit rate achieved was 17 bps when using a single solenoid without the use of a guard interval (Case III). Although one solenoid consumes less energy than two solenoids, it generates weaker and less stable seismic signals. This resulted in lower SNR, and created difficulties in selecting a proper threshold value, and it produced greater BER (Fig. 10d and f; Fig. 10e and b, see also Table 2).

Introducing a guard interval could help solve the inter-byte interference problem, decreasing the BER (Fig. 10b and f; Fig. 10d and e; Table 2). Although the bit rate decreased after applying guard intervals, the energy consumption remained the same because the solenoids were not operated during guard intervals. The performance difference caused by the guard intervals when two solenoids are activated is not as strong as when only one is activated. A possible explanation for this finding is that the amplitude of a pulse induced by a single solenoid may vary, even though it is consistent most of the time (Fig. 7b). When the generated pulse has a relatively large amplitude, the pulse may spread beyond its allotted time, causing it to interfere with neighboring pulses. Even after attenuation, this pulse may still be stronger than other impulses. When two solenoids are used, the generated impulses are more consistent; the resulting SNRs are higher, and the inter-bit interference is less pronounced.

As shown in Table 2, the bit rate was mainly affected by whether or not guard intervals are used, and it was limited by the mechanical operation of the source. When a guard interval of 40 ms was used, the bit rate dropped to 10 bps. With the voltage input of 12 VDC, the measured current when activating a single solenoid was 250 mA, indicating that the power of one solenoid is 3 W. We

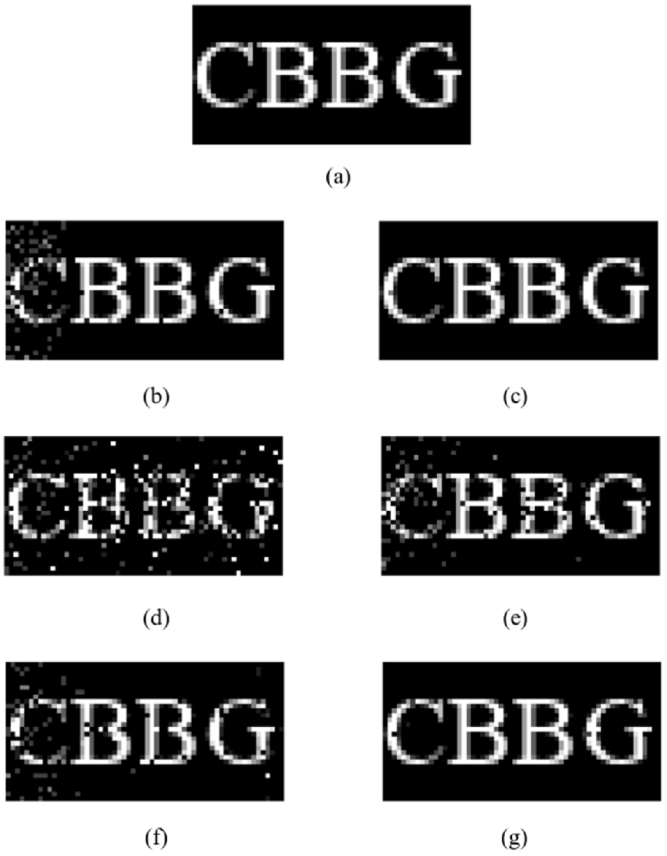

Fig. 10. Comparison of decoded image files: (a) Original image sent through soils; Restored images at the receiver for (b) Case I; (c) Case II; (d) Case III; (e) Case IV; (f) Case V and (g) Case VI.

assumed a 50% duty cycle, i.e. the binary streams contain 50% "1" s and 50% "0" s. Without guard intervals, the power of a single solenoid is estimated as 1.5 W. The power of the vibration source decreased slightly with increase in the guard interval. However, the total energy consumption was not affected by the guard interval. It depended on the number of bits sent as well as the energy consumed to send each bit, which, in turn, depends on the number of solenoids used. With the use of Hamming code, the number of total bits increased; as a result, both the operation time and the energy consumption increased.

4. Discussion

4.1. Practical considerations and cost

In practical applications, the optimal operation mode can be selected based on application requirements. When the accuracy of message transmission is most important, such as the transmission of important data obtained in the field, it is suggested to use both Hamming code and guard intervals to achieve a low BER (Case II). When transmission speed is the primary concern, the guard intervals and the Hamming code can be omitted (Case V). The BER for Case V when transmitting the image was 3.19%. The BER can be further decreased when sending plain text instead of images, by applying spelling correction techniques. The two-solenoid design also enhances the resilience of the system in that the system would still work if one solenoid should fail (Case IV).

Table 1
Controlled parameters for different test cases.

Case	Number of solenoids	Hamming code	Guard interval
I	2	×	✓
II	2	✓	✓
III	1	×	×
IV	1	×	✓
V	2	×	×
VI	2	✓	×

Table 2
Performance characteristics for different test cases.

Case	BER (%)	Bit rate (bps)	Power (W)	Time (min)
I	2.58	10	1.8	12
II	0.1	10	1.8	21
III	8.99	17	1.5	7
IV	3.86	10	0.9	12
V	3.19	16	3	7.5
VI	0.54	16	3	13

The underground communication system developed in this study was built using off-the-shelf components. The total cost of the system was less than US$100 (US$30 for two solenoids, US$10 for one accelerometer, US$22 for one microcontroller, and US$24 for one motor controller). The total cost of the system could be further reduced if the components are purchased or manufactured in bulk.

4.2. Limitations and future work

Because the test setup was limited by the sand tank size, the maximum transmission range of the developed system in dry medium dense sand has not been determined. However, the relatively high SNR and the low path loss indicate that a transmission range of several meters could be achieved. The proposed system was also tested in saturated sand in the laboratory. It worked well but a systematic evaluation needs to be completed to analyze the effect of water content on the system performance. Due to the limitations by mechanical operation of the solenoids and the OOK modulation, the bit rate was less than 20 bps, which can be improved by making further modifications. One potential way to improve the current design is to shorten the gap between the solenoids and the 3D-printed case; this would reduce the travel distance of the plungers, reducing the mechanical operation time. Another potential improvement is to integrate the current communication system into a self-burrowing robot (Tao et al., 2020). Similar to mole-rats which rely on their heads and feet to burrow as well as to generate seismic signals, it is possible that vibrations used for data transmission may be generated during the robotic burrowing process. Robotic integration could also be more cost-effective and energy efficient, as no extra energy is required for communication specifically; the installation cost could also be reduced since the sources and sensors are integral parts of the robots; furthermore, the source and sensor nodes are mobile instead of static, allowing a reconfigurable dynamic underground IoT network to be established.

5. Conclusions

In this study, an underground wireless communication system based on vibration was developed. Two vibrational sources, one inspired by biological tremulation and the other by drumming, were designed and fabricated using off-the-shelf components. It

was found that the drumming-inspired source generated vibrational signals with higher acceleration amplitudes and higher SNR. Text files and image files were first encoded into binary streams with the option of using Hamming code for error correction. The binary streams were then used to control the on/off state of the source, and optional guard intervals were introduced between bytes. The resulting vibrations were measured using an MEMS accelerometer, and the signals were decoded to restore the information. The plain text file was perfectly restored, while the BER for the image transmission was as low as 0.1%. In general, the implementation of the Hamming code and guard intervals decreased the bit error ratio and bit rate while increasing the power consumption and operation time; using two solenoids instead of one in the drumming-inspired source further decreased the bit error ratio and enhanced the resilience of the system but increased the power and operation time. The proposed system can effectively transmit information as far as 80 cm in the laboratory in dry medium dense sand. Future large-scale and field-scale tests are needed to further evaluate the performance of the proposed system in different types of soils and under different soil conditions.

Declaration of competing interest

The authors declare that they have no known competing financial interests or personal relationships that could have appeared to influence the work reported in this paper.

Acknowledgements

This material is based upon work primarily supported by the National Science Foundation (NSF) (Grant No. EEC-1449501). Any opinions, findings and conclusions, or recommendations expressed in this paper are those of the author(s) and do not necessarily reflect those of NSF.

References

Akyildiz, I.F., Stuntebeck, E.P., 2006. Wireless underground sensor networks: research challenges. Ad Hoc Netw. 4 (6), 669–686.
Auersch, L., 2010. Technically induced surface wave fields, Part I: measured attenuation and theoretical amplitude-distance laws. Bull. Seismol. Soc. Am. 100 (4), 1528–1539.
Auersch, L., Said, S., 2010. Attenuation of ground vibrations due to different technical sources. Earthq. Eng. Eng. Vib. 9 (3), 337–344.
Bruchanov, M., 2005. BruXy: radio teletype communication. http://bruxy.regnet.cz/web/hamradio/EN/r.teletype-communication/. Accessed May 2022.
Cocroft, R.B., Gogala, M., Hill, P.S.M., Wessel, A., 2014. Studying Vibrational Communication. Springer, Berlin.
Ema, M.H., 2012. Vibrational Communication of Subterranean Rodents. PhD Thesis. University of South Bohemia, České Budějovice, Czech.
Heth, G., Frankenberg, E., Raz, A., Nevo, E., 1987. Vibrational communication in subterranean mole rats (Spalax ehrenbergi). Behav. Ecol. Sociobiol. 21, 31–33.
Hill, P.S.M., 2001. Vibration and animal communication: a review. Am. Zool. 41 (5), 1135–1142.
Hill, P.S.M., Lakes-Harlan, R., Mazzoni, V., Narins, P.M., Virant-Doberlet, M., Wessel, A., 2019. Biotremology: Studying Vibrational Behavior. Springer, Berlin.
Ikrath, K., Schneider, W., 1968. Communications via seismic waves employing 80-Hz resonant seismic transducers. IEEE Trans. Commun. 16 (3), 439–444.
Lin, S.C., Alshehri, A.A., Wang, P., Akyildiz, I.F., 2017. Magnetic induction-based localization in randomly deployed wireless underground sensor networks. IEEE Internet Things J. 4 (5), 1454–1465.
Narins, P.M., Reichman, O.J., Jennifer, U.M.J., Lewis, E.R., 1992. Seismic signal transmission between burrows of the Cape mole-rat, Georychus capensis. J. Comp. Physiol. 170, 13–21.
Nevo, E., Heth, G., Pratt, H., 1991. Seismic communication in a blind subterranean mammal: a major somatosensory mechanism in adaptive evolution underground. Proc. Natl. Acad. Sci. USA 88 (4), 1256–1260.
O'Connell-Rodwell, C.E., 2007. Keeping an "Ear" to the ground: seismic communication in elephants. Physiology 22 (4), 287–294.
Ohmura, W., Takanashi, T., Suzuki, Y., 2009. Behavioral analysis of tremulation and tapping of termites (Isoptera). Sociobiology 54 (1), 269–274.
Rado, R., Levi, N., Hauser, H., et al., 1987. Seismic signalling as a means of communication in a subterranean mammal. Anim. Behav. 35 (4), 1249–1251.
Ramesh, M.V., 2014. Design, development, and deployment of a wireless sensor network for detection of landslides. Ad Hoc Netw. 13, 2–18.
Raza, U., Salam, A., 2020. Wireless underground communications in sewer and stormwater overflow monitoring: radio waves through soil and asphalt medium. Information 11 (2), 98.
Saeed, N., Alouini, M.S., Al-Naffouri, T.Y., 2019. Toward the internet of underground things: a systematic survey. In: IEEE Commun. Surv. Tut, vol. 21, pp. 3443–3466.
Salam, A., Shah, S., 2019a. Internet of things in smart agriculture: enabling technologies. In: 2019 IEEE 5th World Forum on Internet of Things (WF-IoT), Limerick, Ireland, pp. 692–695.
Salam, A., Shah, S., 2019b. Urban underground infrastructure monitoring IoT: the path loss analysis. In: In: 2019 IEEE 5th World Forum on Internet of Things (WF-IoT), Limerick, Ireland, pp. 398–401.
Santamarina, J.C., Klein, K.A., Fam, M.A., 2001. Soils and Waves. J. Wiley & Sons, New York, USA.
Stokoe, K.H., Santamarina, J.C., 2000. Seismic-wave-based testing in geotechnical Engineering. In: ISRM International Symposium, Melbourne, Australia.
Sun, Z., Akyildiz, I.F., 2010a. Channel modeling and analysis for wireless networks in underground mines and road tunnels. IEEE Trans. Commun. 58 (6), 1758–1768.
Sun, Z., Akyildiz, I.F., 2010b. Magnetic induction communications for wireless underground sensor networks. IEEE Trans. Antenn. Propag. 58 (7), 2426–2435.
Tao, J.L., Huang, S.C., Tang, Y., 2020. SBOR: a minimalistic soft self-burrowing-out robot inspired by razor clams. Bioinspiration Biomimetics 15 (5), 055003.
Vuran, M.C., Salam, A., Wong, R., Irmak, S., 2018a. Internet of underground things: sensing and communications on the field for precision agriculture. In: In: 2018 IEEE 4th World Forum on Internet of Things (WF-IoT), Singapore, pp. 586–591.
Vuran, M.C., Salam, A., Wong, R., Irmak, S., 2018b. Internet of underground things in precision agriculture: architecture and technology aspects. Ad Hoc Netw. 81, 160–173.
Yang, S.J., Baltaji, O., Singer, A.C., Hashash, Y.M.A., 2020. Development of an underground through-soil wireless acoustic communication system. IEEE Wireless Commun. 27 (1), 154–161.
Zhong, Y., Gao, Y.Q., Tao, J.L., 2021. Bio-inspired underground communication using seismic waves. In: IFCEE 2021, Minneapolis, United States, pp. 139–148.

Dr. Junliang (Julian) Tao is an associate professor in the School of Sustainable Engineering and the Built Environment at Arizona State University. He also serves as a Senior Investigator at the National Science Foundation Engineering Center for Bio-mediated and Bio-inspired Geotechnics (CBBG). He holds a Bachelor's degree from China University of Geosciences (Wuhan), a Master's degree from Tongji University, and a Ph.D. degree from Case Western Reserve University. His research area includes bio-inspired self-burrowing robots, bio-inspired underground sensing and communication, and bio-inspired sustainable countermeasures to natural hazards. He serves on the editorial board of American Society of Testing Materials (ASTM) Journal of Testing and Evaluation and serves on committees in American Society of Civil Engineers (ASCE), Transportation Research Board (TRB), Society of Photo-Optical Instrumentation Engineers (SPIE), and the Institute of Electrical and Electronics Engineers (IEEE). Dr. Tao is the recipient of the (US) National Science Foundation CAREER Award in 2017. He was also awarded the Young Civil Engineer of the Year in 2017 by the ASCE Akron-Canton Section for "promoting professionalism and the advancement of the civil engineering profession".